CASMO-5 95/95 Tolerance Limits for measured reactivity decrement biases of the EPRI/Studsvik Burnup Benchmark

Following discussions with the NRC Staff at the NRC/EPRI/NEI public meeting (June 8, 2016: ML16146A035), EPRI has now implemented a purely statistical approach for interpreting the 95/95 tolerance limits on the burnup dependence of the Hot Full Power (HFP) decrement bias by directly using 95% prediction intervals of regression fits. Unlike previous EPRI methods employed, this statistical approach lumps all measurement uncertainties into the derived 95/95 tolerance limits. This approach produces limits that contain significant contributions from measurement uncertainties, and these 95/95 tolerance limits are more conservative than the regression confidence limits derived from earlier EPRI analyses.

This memo provides a summary of the updated statistical analysis of 95/95 tolerance limits for the measured Hot Full Power (HFP) PWR fuel reactivity depletion decrement biases derived from Duke reactor data, as documented in EPRI Technical Report 1022909 [1]. This memo also discusses the rollup of uncertainties used to obtain the final cold reactivity depletion decrement bias uncertainties that will be included in the soon-to-be-revised EPRI Burnup Benchmark report.

Summary of the Analysis Procedure

The steps in the overall procedure to compute statistical confidence limits for the reactivity decrement bias curves derived using the EPRI methodology and measured data are:

1. Generate a master database (for all 2856 HFP sub-batch data of the original EPRI report) that contains: a unique sub-batch/cycle index, the sub-batch burnup, the sub-batch sensitivity, and the sub-batch reactivity decrement bias.

2. Plot the reactivity decrement bias versus sub-batch sensitivity and perform a quadratic regression to determine the 95% prediction interval for the reactivity decrement bias versus sub-batch sensitivity.

3. Approximate the individual sub-batch reactivity decrement bias sensitivity variances from the spread of the 95% prediction interval curves (of the reactivity decrement bias regression vs. sub-batch sensitivity) by using the individual sub-batch sensitivities.

4. Determine the burnup variance of individual reactivity decrement bias points from a quadratic function of bias versus sub-batch burnup, and combine this reactivity decrement bias burnup variance with the sub-batch sensitivity variance to get a total variance estimate for each of the 2856 data points.

5. Determine the additional component of bias and uncertainty that accounts for intra-batch burnup distribution effects and corrects for assumption that reactivity decrements are computed from batch-averaged burnups.

6. Collect all 2856 HFP reactivity decrement biases and collapse the data within individual sub-batch/cycles to one average value of reactivity decrement bias by statistically combining data using individual data variances. (This is the assumption of 100% correlation within a sub-batch/cycle.)

7. Perform a Weighted Least Squares (WLS) nonlinear regression fit to the collapsed reactivity decrement bias versus sub-batch burnup, and compute 95% confidence and prediction intervals for the regression fit.

8. Perform a Shapiro-Wilk test to determine if the data "passes the normality test," so that confidence and prediction intervals can be correctly interpreted in deriving tolerance limits.

9. Multiply the 95% prediction intervals by the ratio of the one-sided Tolerance Limit Factor for (95%, 95%, # sub-batch/cycles) to the Student's t-value for (95%, # of sub-batch/cycles) to estimate the 95/95 Tolerance Limits. This step is necessary since we seek a 95/95 confidence limit on the regression fit to reactivity decrement bias. Note that the Student's t-value is used in constructing regression confidence intervals, and this relies on the fact that the underlying distribution of residuals is Gaussian.

10. Combine the HFP 95/95 tolerance limit of HFP reactivity decrement bias uncertainties with the fuel temperature and Hot-to-Cold uncertainties to obtain the final uncertainties to be aplied to the EPRI cold benchmark lattices.

Implementation of the Analysis Procedure

Step 1 was implemented to generate a new master database that contains: a unique sub-batch/cycle index, the sub-batch burnup, the sub-batch sensitivity, and the sub-batch reactivity decrement bias. This database contains 2856 reactivity decrement biases as derived from the summary files of the 3 million CASMO-5/SIMULATE-3 cases that were run for the original EPRI/Studsvik report. Figure 1 displays the unfiltered individual data points for high and low enrichment sub-batches and 5% reactivity decrement (e.g., Kopp) bounds at HFP.

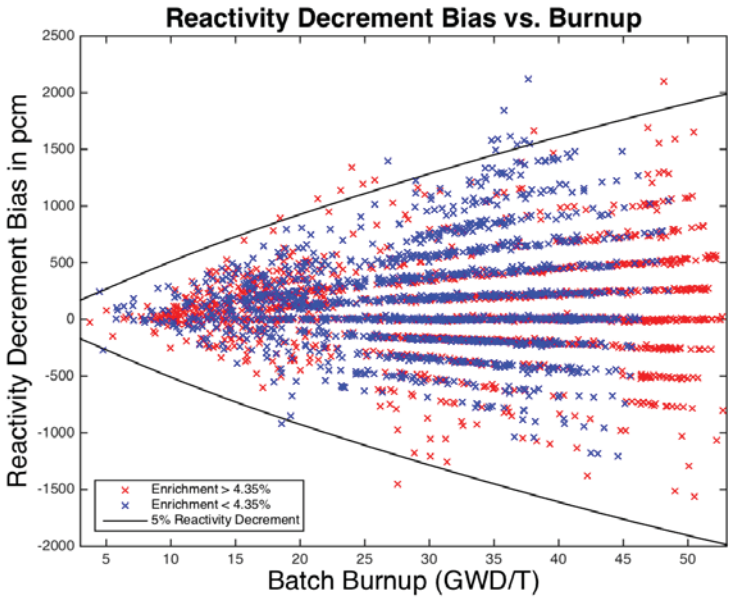

Figure 1 Measured Casmo-5 Reactivity Decrement Biases vs. Sub-batch Burnup

For Steps 2-3 of the analysis, reactivity decrement bias data was plotted vs. sub-batch sensitivity, and a quadratic regression was performed to determine the 95% prediction interval for the reactivity decrement bias versus sub-batch sensitivity, as displayed in Figure 2. The 95% prediction interval was used to compute the normalized shape of 2-sigma variation versus sensitivity. The square of this variation (the variance) was fit to a quadratic polynomial and normalized as displayed in Figure 3. The data was fitted only up to a sensitivity of 4.0%, as the data becomes exceedingly sparse at the higher sensitivity end of the data. The plus signs in this figure are variance points as determined using the Matlab VAR function for eight separate sub-batch sensitivity bins - to verify that the quadratic fit was reasonable.

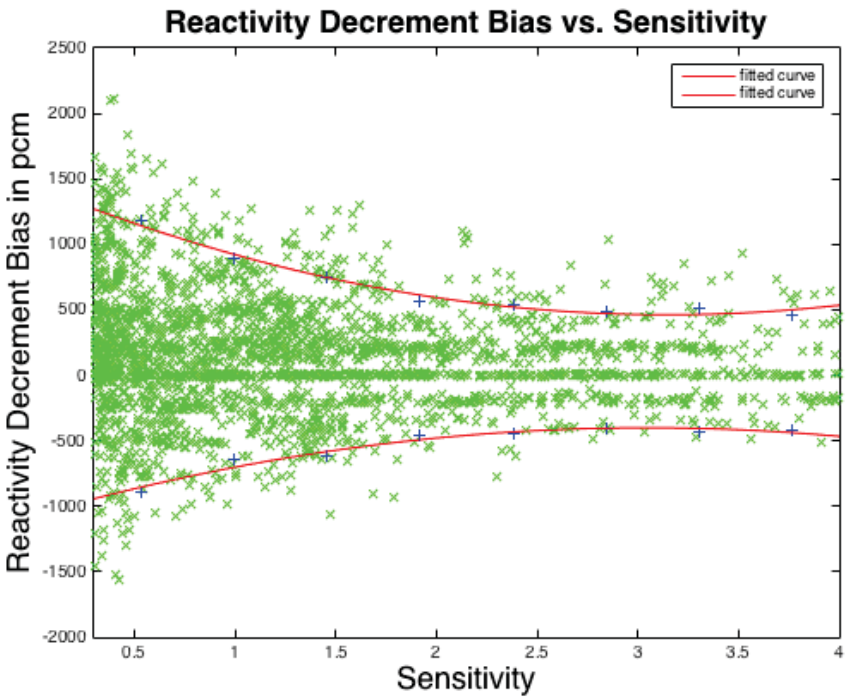

Figure 2 Reactivity Decrement Bias vs. Sub-batch Sensitivity

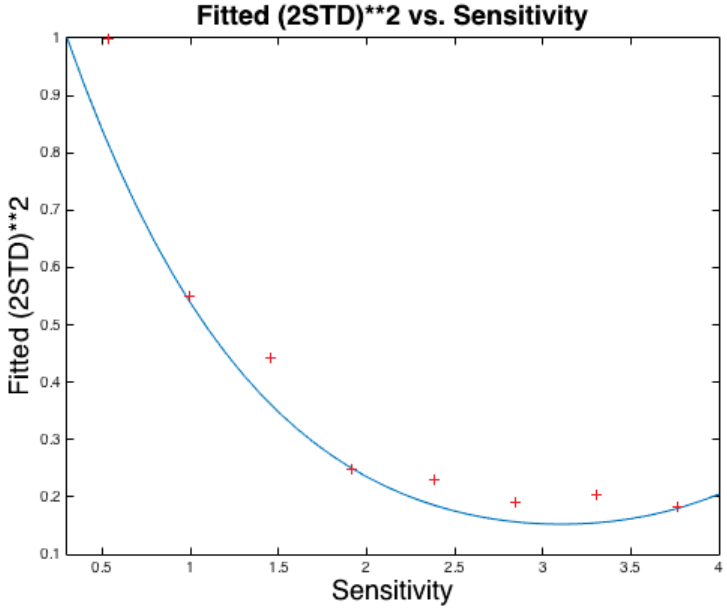

Figure 3 Reactivity Decrement Quadratic Fit vs. Sub-batch Sensitivity

For Step 4 of the analysis, reactivity decrement bias data (without the additional screening used in previous EPRI analyses) was plotted vs. sub-batch burnup and a quadratic regression was performed to determine the 95% prediction interval for the reactivity decrement bias versus sub-batch burnup, as displayed in Figure 4. The fitted 95% prediction interval was used to compute the shape of 2-sigma variation versus burnup, and the square of this variation (the variance) was fit to a quadratic polynomial and renormalized as displayed in Figure 5. This figure also contains variance points, as determined using the Matlab VAR function for fifteen separate sub-batch burnup bins - to verify that the quadratic fit was reasonable.

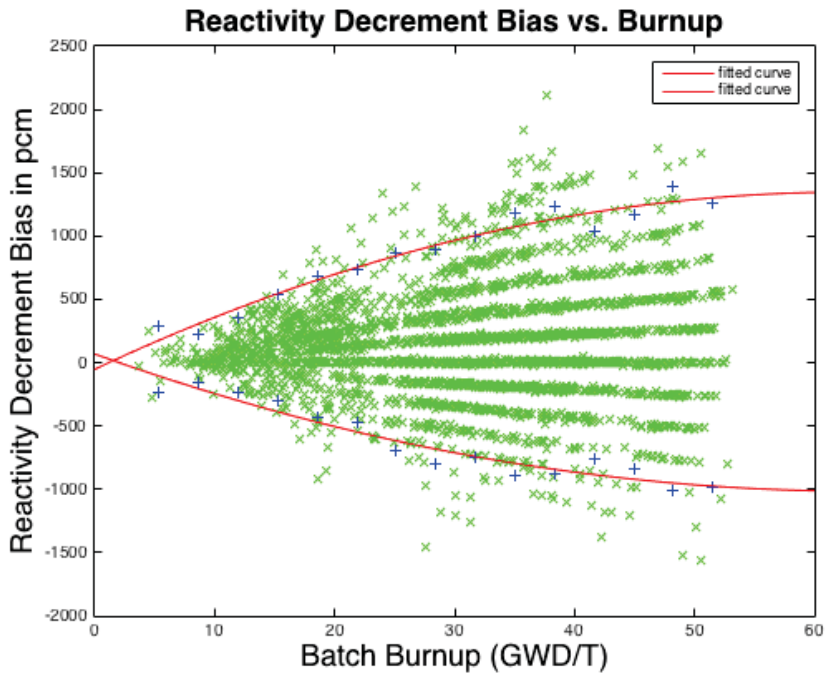

Figure 4 Reactivity Decrement Bias vs. Sub-batch Burnup

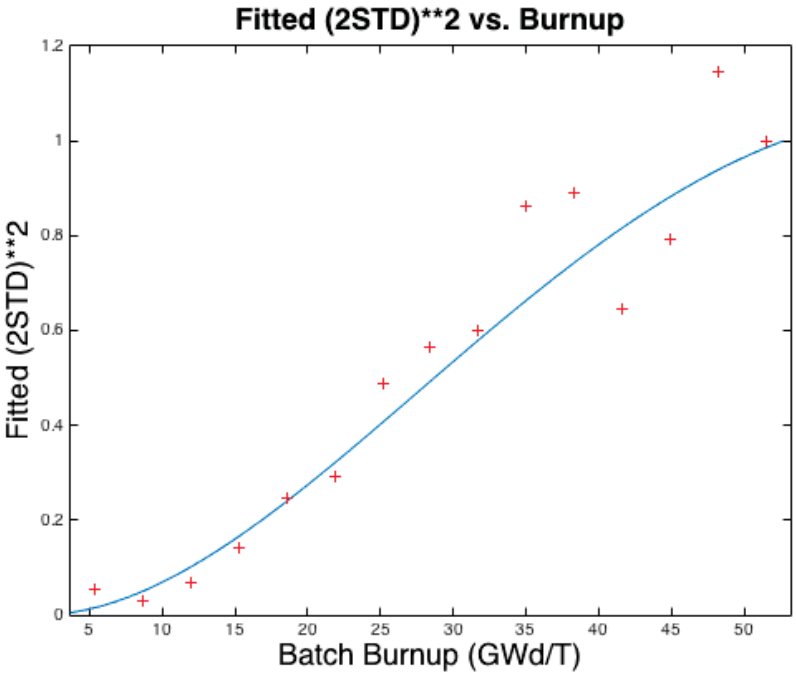

Figure 5 Reactivity Decrement Quadratic Fit vs. Sub-batch Burnup

Weights for each of the 2856 data points were computed by combining the two reciprocals of fitted variances evaluated with the sub-batch sensitivity and the burnup of each of the data point. Two methods for computing weights were evaluated,

$$W_i = \frac{1}{\sigma^2(S_i)} + \frac{1}{\sigma^2(B_i)} \quad and \quad W_i = \frac{1}{\sigma^2(S_i)} \cdot \frac{1}{\sigma^2(B_i)}$$

There was little difference between regression fits and prediction intervals computed using these two variance estimation procedures. However, the product formulation was selected for all regression analysis based on the fact that it correctly produces zero weight should either the sensitivity or burnup term goes to zero, and the additive formulation does not. **Weighted Least Squares (WLS) fitting of data without any sensitivity or burnup screening was then performed** (unlike the 0.9% sensitivity screening and 10.0 GWd/T burnup screening used in the original EPRI analysis). This change was made for two reasons:

1) WLS regressions are not significantly affected by the low sensitivity data points (unlike Ordinary Least Square (OLS) analysis) and,
2) This approach eliminates the previous NRC concerns about **potential influence of data screening** on the resulting regression biases and derived uncertainties.

All regression fits versus burnup were performed using the MATLAB *nlinfit* function with the '*weight'* option to use the individual data weights, computed as described above. Confidence intervals corresponding to each data point were computed using the MATLAB *nlpredci* function with *'Covar'*, and '*weight'* options. Confidence interval curves as a function of burnup were computed using MATLAB *polyfit* function to fit individual confidence interval data to 6-th order polynomials. Prediction intervals corresponding to each data point were computed using the MATLAB *nlpredci* function with *'Covar'*, *'predopt' 'observation'*, and '*weight'* options. Prediction interval curves as a function of burnup were computed using MATLAB *nlinfit* function to fit individual prediction interval data to quadratic polynomials - constrained to a value of 0.0 at 0.0 GWd/T burnup.

Figures 6 and 7 display MATLAB OLS and WLS quadratic regressions with confidence interval and prediction intervals curves, respectively.

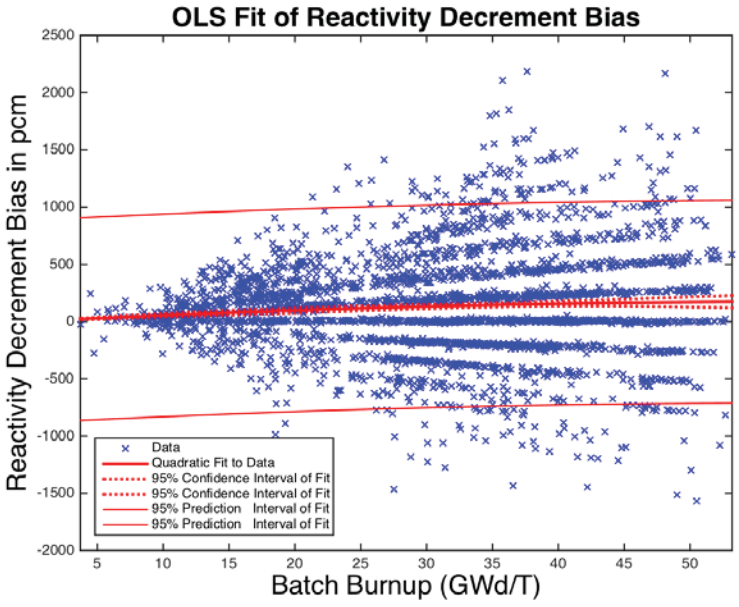

Figure 6 Reactivity Decrement Quadratic OLS Regression vs. Sub-batch Burnup

Despite large differences in the weight functions, both OLS and WLS regressions produce similar fits for the decrement bias. The fact that weights have little impact on regression fits implies that measured reactivity decrement biases are not sensitive to estimates of the dependence of variance on sub-batch burnup and sensitivity. However, prediction intervals of WLS regressions are narrower than those of the OLS regressions. This implies

that many of the widely spread data points have low sensitivities, and consequently the weighting in WLS regressions significantly decreases their contribution to regression prediction intervals.

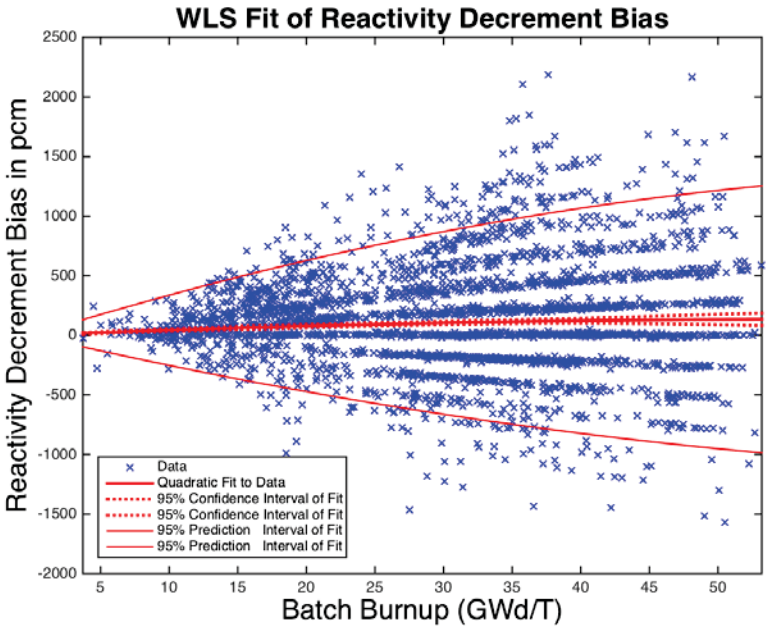

Figure 7 Reactivity Decrement Quadratic WLS Regression vs. Sub-batch Burnup

The Step 5 correction for computing reactivity decrement biases from batch-averaged burnups was implemented by: 1) evaluating the maximum value of the second derivative of reactivity within each sub-batch/cycle burnup range, 2) multiplying this second derivative by the maximum difference of any assembly burnup from the sub-batch average burnup, and 3) multiplying this result by the sub-batch average burnup change ($E_M - E_{ave}$) determined in the U^{235} fission distribution r.m.s. minimization. The sub-batch bias and sub-batch bias addition are depicted schematically in Figure 8 for a hypothetical sub-batch of three assemblies having burnup E_1, E_2, and E_3.

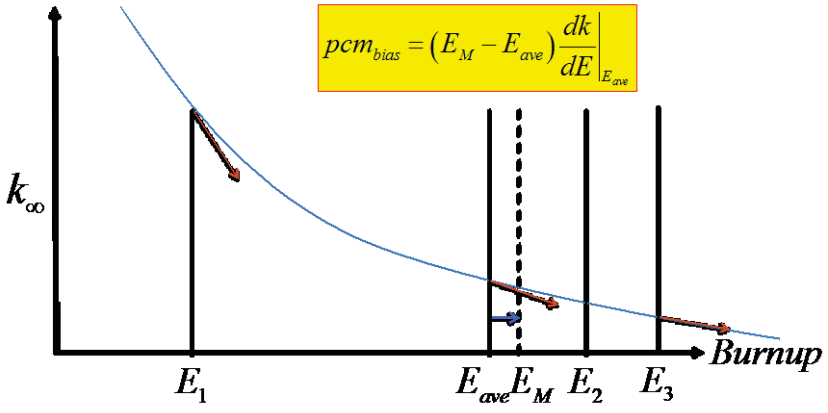

Figure 8 Reactivity Decrement Corrections for Sub-Batch Burnup Distributions

These reactivity decrement bias additions for all data points are displayed in Figure 9. The magnitude of these corrections is very small for most data points because either the slope of reactivity is nearly constant within the range of batch burnup within a cycle, or because the range of intra-batch burnup is very small. When considering all sub-batch data points, the average of the maximum deviation of intra-batch burnup from the sub-batch average burnup is 2.0 GWd/T in absolute units and 6.6% in relative terms – not very large. (Note that if the derivative of k-infinity were independent of burnup, the intra-sub-batch burnup distribution would require no additional correction to the bias.) The implementation of this correction included three additional conservatisms:

1) The second derivative of reactivity was evaluated at its maximum anywhere in the sub-batch/cycle.
2) The intra-batch burnup difference was taken as the maximum value within the sub-batch – even when it corresponds to only a single assembly of all the assemblies within the sub-batch.
3) The sign of the addition to each reactivity decrement bias was selected to maximize the absolute value of reactivity decrement bias (e.g., positive biases are increased and negative biases are decreased).

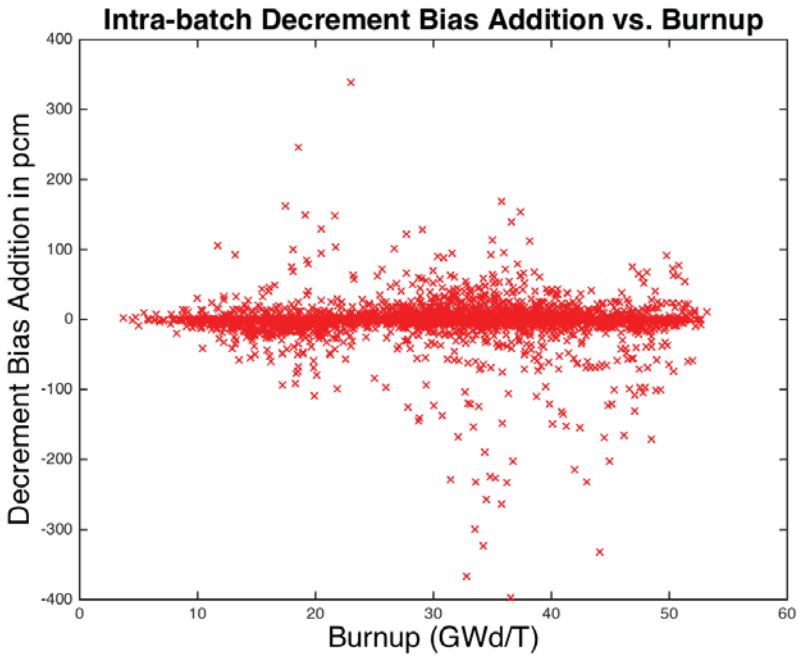

Figure 9 Intra-batch Reactivity Decrement Bias Addition vs. Sub-batch Burnup

Step 6 was implemented by collapsing all data within individual sub-batch/cycles to one average value per cycle by statistically combining individual reactivity decrement biases and burnups with their respective weights (i.e., the reciprocal variances product). This is the assumption of 100% correlation of data within each sub-batch/cycle that is necessary so regression fit confidence intervals can be applied correctly (given that we cannot know the precise intra-cycle correlation of data that would be needed to use individual data point regressions). When collapsed over each cycle, there are 270 sub-batch/cycle reactivity decrement bias points available for the subsequent analysis. Two different methods for collapsing the sub-batch/cycle decrement bias data were examined: 1) un-weighted collapsing and 2) collapsing with individual data point weights. Figure 10 displays un-collapsed and collapsed reactivity decrement bias data for nine typical sub-batch/cycles. The **plus sign** symbols represent burnup points of **un-collapsed data**, the **square** symbols represent **un-weighted** collapsed points, and **circle** symbols represent the **weighted** collapsed points. By examining data for separate colors (i.e., sub-batches) it can be seen that weighted and un-weighed collapsed data differ very little in reactivity decrement bias and only slightly more in collapsed burnup. As might be expected, regression analysis was shown to be extremely

insensitive to the collapsing method employed, so the more intuitive **weighted collapse** was selected for all subsequent regression analysis.

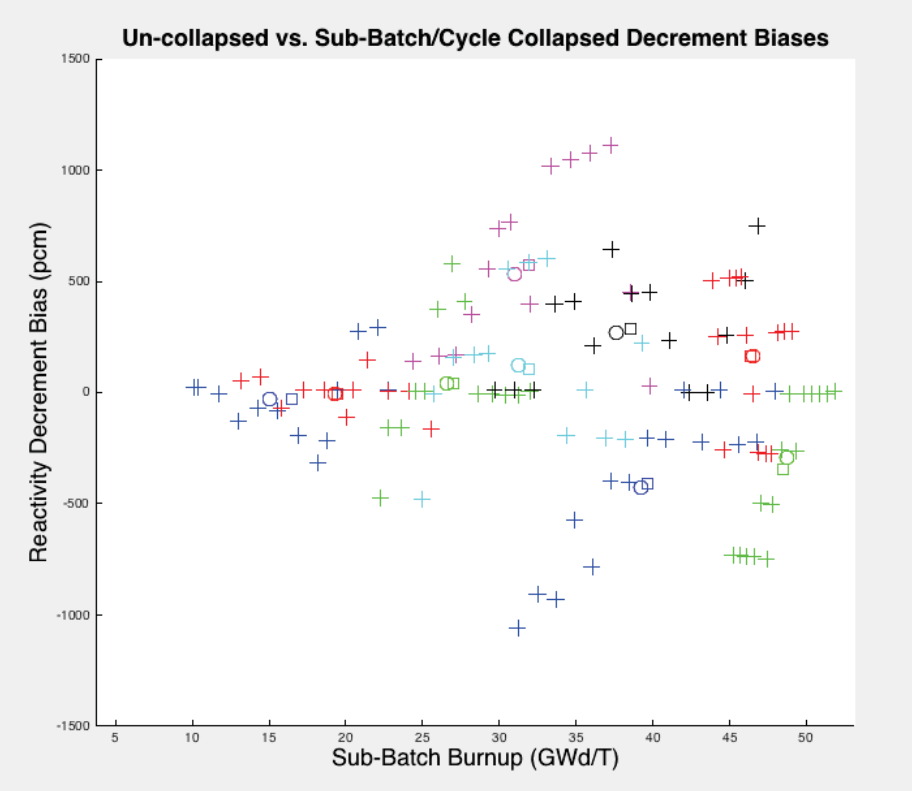

Figure 10 Cycle-collapsed Reactivity Decrement Data

An OLS quadratic regression fit of the sub-batch/cycle-collapsed data is displayed in Figure 11. Note that the data tends to separate into three clusters that represent the fresh, once-burned, and twice-burned fuel sub-batches.

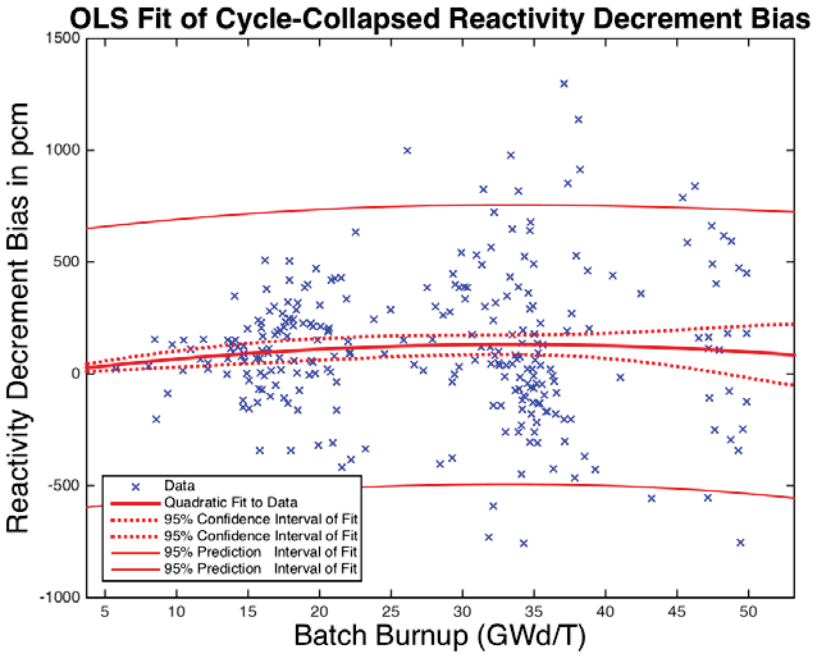

Figure 11 Reactivity Decrement Quadratic OLS Regression For Cycle-collapsed Data

For Step 7, these sub-batch/cycle collapsed decrement bias data were used in a Weighted Least Squares (WLS) quadratic regression fit, as displayed in the Figure 12. Note the prediction intervals are narrower than those obtained in the previous un-collapsed WLS regression of the 2856 individual data points, as displayed in Figure 7.

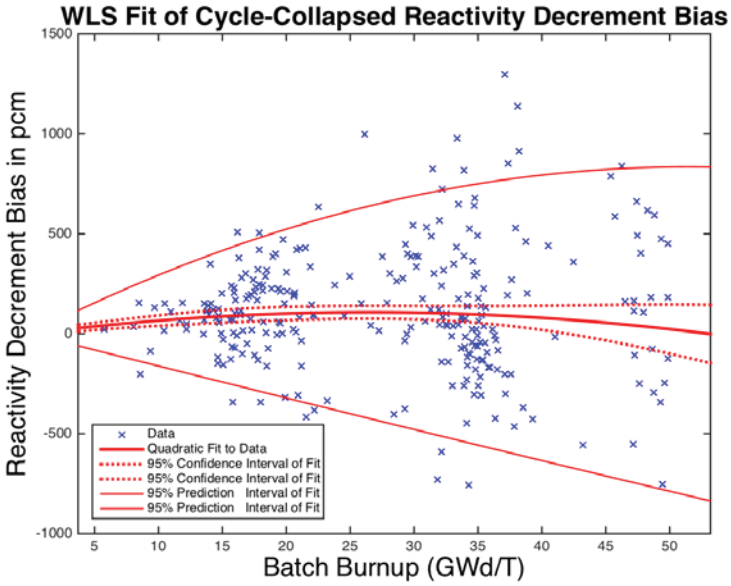

Figure 12 Reactivity Decrement Quadratic WLS Regression For Cycle-collapsed Data

The shape of the prediction interval bounds in Figure 12 appears to deviate from the "cone" shape of previous figures because of the parabolic shape of the regression fit, but the prediction interval width remains similar. This is clearer in Figure 13, where **linear** WLS regression results are displayed, and the prediction interval appears more conical. Note in the linear regression, the confidence interval is narrower than that of the quadratic regression of Figure 12. However, we still chose to subsequently use quadratic regressions because it is important to allow for a regression shape that could have an asymptotic value at large burnups - where isotopic inventories of the fuel assemblies become more constant (e.g., U^{235} is nearly depleted and Pu^{239} becomes nearly constant).

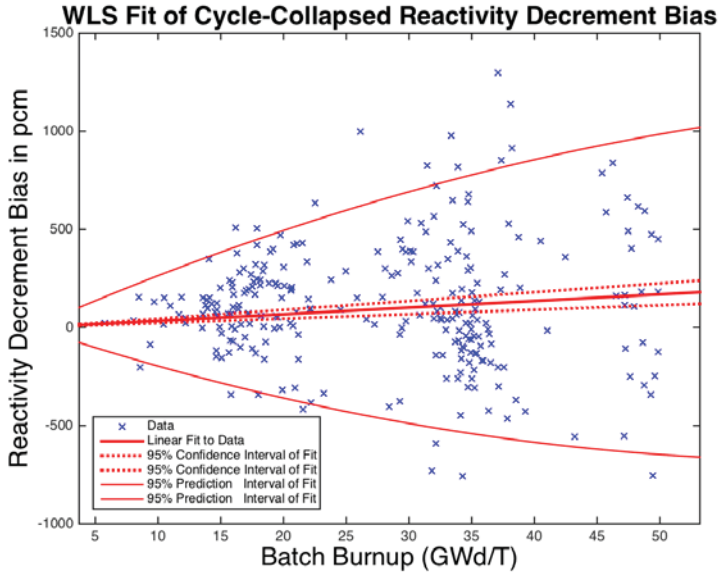

Figure 13 Reactivity Decrement Linear WLS Regression For Cycle-collapsed Data

For Step 8, the standardized residuals (differences between the data points and the quadratic regression fit divided by the square root of the variance of each data point) were used in a Shapiro-Wilk test (using the StatPlus Excel add-on) to determine if the data "passes the normality test," as is required for confidence intervals to be correctly applied to the regression fits. As can be seen from the results in Figure 14, the residuals pass the Shapiro-Wilk normality test, as well as the Kolmogorov-Smirnov/Lilliefor and D'Agostino normality tests.

The data from the quadratic regression fit of Figure 12 are summarized in Table 1, and one can observe that the maximum width of the 95% confidence and prediction intervals are 190 pcm and 875 pcm at high burnup. The important point to recall here is that because the sub-batch/cycle data points having been compressed to a single value, there are no correlation effects between successive flux map measurement points to be considered. Consequently, the regression confidence and prediction interval widths can be justifiably used - since the residuals correspond to a normal distribution, a condition that is needed for inferring the 95% confidence and prediction intervals for regression fits. Data from the linear regression fit of Figure 13 are also summarized in Table 1, and the maximum widths of the 95% confidence and prediction intervals are 67 pcm and 879 pcm.

Normality Tests

Variable #1 (Reactivity Decrement Bias Residuals)

Sample size	**270**	***Mean***	**8.82425**
Standard Deviation	**225.28857**	***Median***	**0.**
Skewness	**0.01589**	***Kurtosis***	**2.74747**
Skewness (Fisher's)	**0.01598**	***Kurtosis (Fisher's)***	**-0.23471**

	Test Statistics	*p-level*	*Conclusion: (5%)*
Kolmogorov-Smirnov/Lilliefor Test	**0.02319**	**0.97833**	***No evidence against normality***
Shapiro-Wilk W	**0.99461**	0.45792	*Accept Normality*
D'Agostino Skewness	**0.10939**	**0.91289**	***Accept Normality***
D'Agostino Kurtosis	**-0.78382**	**0.43315**	***Accept Normality***
D'Agostino Omnibus	**0.62633**	**0.73113**	***Accept Normality***

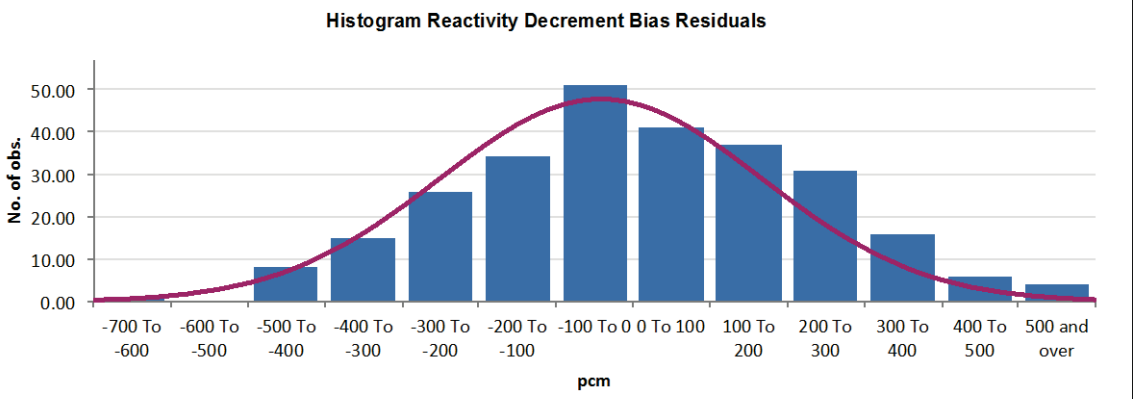

Figure 14 Normality Tests of Cycle-Collapsed WLS Regression Residuals of Figure 12 Data

For Step 9, the prediction intervals are multiplied by the ratio of the two-sided 95/95 Tolerance Limit Factor (for the 95% Student's t-value for 270 sub-batch/cycles data points) to obtain the 95/95 Tolerance Limits. Since there are 270 data points, this ratio is 1.074, and differences between prediction intervals and tolerance limits are not large - given the large number of data points. Note that the Student's t-value is used in constructing regression prediction intervals, and here one makes use of the fact that the underlying distribution of residual biases is Gaussian – as shown by the Shapiro Wilk test.

Table 1 Summary of WLS Regression Biases, Confidence Intervals, and Prediction Intervals

Depletion Reactivity Decrement Regression Parameters (pcm)						
Burnup (GWd/T)	Quadratic Regression			Linear Regression		
	Bias	C.I. Width	P.I. Width	Bias	C.I. Width	P.I. Width
10	66	26	226	34	11	228
20	101	33	420	67	22	426
30	106	33	585	101	34	590
40	80	60	713	135	44	719
50	22	123	812	169	56	817
60	-64	190	875	203	67	879

Final Analysis for Cold Reactivity Decrement Uncertainties

For Step 10, the HFP reactivity decrement bias prediction intervals must be statistically combined with the fuel temperature and Hot-to-Cold uncertainties. In Table 8-1 of the original EPRI report [1] a very conservative approach to the fuel temperature uncertainty was taken by statistically combining the maximum instantaneous fuel temperature difference (150 pcm) and the maximum historical fuel temperature difference (206 pcm) to arrive at a combined fuel temperature uncertainty of 255 pcm – that was then applied independent of burnup. This approach leads to an extremely conservative uncertainty for low burnups, because the reactivity decrement uncertainty must physically go to 0.0 pcm at zero burnup. Consequently, it is more appropriate to statistically combine the two fuel temperature uncertainties at each burnup step to obtain a more realistic uncertainty as a function of burnup. Table 8-1 of the original EPRI report [1] has been augmented in the following table with the right-most column that contains the combined fuel temperature **uncertainty as a function of burnup**. At 10.0 GWd/T, the uncertainty is reduced to 146 pcm rather than the conservative 255 pcm previously used in the previous EPRI analysis.

Table 8-1 Fuel Temperature Effect on Hot and Cold Lattice Reactivity							
	Hot Depletion (HFP)			Branch to Cold (Bor=0, Xen=0, 293K)			Combined
Burnup (GWd/T)	k-infinity (946K)	k-infinity (897K)	Difference 946K - 897K	k-infinity (from 946K)	k-infinity (from 897K)	Difference 946K - 897K	uncertainty (pcm)
0	1.07712	1.07848	-0.00136	1.15285	1.15285	0.00000	136
10	1.13346	1.13492	-0.00146	1.20192	1.20189	0.00003	146
20	1.13467	1.13617	-0.00150	1.21248	1.21229	0.00019	151
30	1.08533	1.0865	-0.00117	1.16481	1.16421	0.00060	131
40	1.02515	1.02586	-0.00071	1.09975	1.09866	0.00109	130
50	0.96862	0.96887	-0.00025	1.03605	1.03445	0.00160	162
60	0.91905	0.91888	0.00017	0.97875	0.97669	0.00206	207

The Hot-to-Cold additional uncertainty that was computed conservatively in the original EPRI report by statistically decomposing the maximum total uncertainty of any lattice burnup step (555 pcm in Table 8-7) from the minimum zero burnup uncertainty of any lattice (322 pcm in Table 8-7) to arrive at a Hot-co-Cold additional uncertainty of 452 pcm. (Recall that the Hot-to-Cold additional uncertainty must be 0.0 at zero burnup because the zero burnup uncertainty for LAR applications uses experimental cold critical uncertainties.)

This additional hot-to-cold uncertainty of 452 pcm computed with TSUNAMI was also applied independent of burnup in the original EPRI analysis. The top portion of Table 2 displays the actual additional hot-to-cold

uncertainties for each of the five lattices of the original EPRI report and it can be observed that uncertainties at low burnups are significantly smaller than the 452 pcm originally employed.

Table 8-7 HFP to Cold Uncertainty Matrix (2-sigma) at Cold Conditions

		Burnup (GWd/T)							
		0	0.5	10	20	30	40	50	60
Base	Reactivity (pcm)	9867	11843	11425	12605	13919	14986	15891	16527
	Uncertainty	347	427	459	508	527	530	521	509
128 IFBA 24 WABA	Reactivity (pcm)	9977	11927	11367	12556	13916	15009	15888	16612
	Uncertainty	337	403	450	508	533	531	521	512
3.50 % Enrichment	Reactivity (pcm)	12703	14810	13078	14402	15525	16266	16734	17034
	Uncertainty	365	437	498	555	550	537	518	500
4.25 % Enrichment	Reactivity (pcm)	11069	13112	12209	13469	14747	15699	16415	16931
	Uncertainty	350	434	473	529	540	534	520	508
Small Fuel Radius	Reactivity (pcm)	10205	12262	11602	12658	13981	14991	15849	16473
	Uncertainty	322	402	442	497	524	518	509	492

Table 2 Hot-to-Cold Additional Uncertainties

	Burnup (GWd/T)							
	0	0.5	10	20	30	40	50	60
	Additional Uncertainty (Referenced to 0.0 GWd/T)							
Base	0	249	300	371	397	401	389	372
128 IFBA 24 WABA	0	221	298	380	413	410	397	385
3.50 % Enrichment	0	240	339	418	411	394	368	342
4.25 % Enrichment	0	257	318	397	411	403	385	368
Small Fuel Radius	0	241	303	379	413	406	394	372
	Additional Uncertainty (Referenced to 0.5 GWd/T)							
Base	-	0	168	275	309	314	299	277
128 IFBA 24 WABA	-	0	200	309	349	346	330	316
3.50 % Enrichment	-	0	239	342	334	312	278	243
4.25 % Enrichment	-	0	188	302	321	311	286	264
Small Fuel Radius	-	0	184	292	336	327	312	284
	Maximum Additional Uncertainty (Referenced to 0.5 GWd/T)							
Max Uncertainty (pcm)	-	-	200	342	349	346	330	316

The top blue curve in Figure 15 displays a plot of the 128 IFBA/24 WABA lattice additional uncertainties as a function of burnup when referenced to zero burnup. The large jump from 0.0 to 0.5 GWd/T burnup occurs in part because of the ~3000 pcm reactivity arising from Xe^{135} in the HFP depleted lattices. Xenon must be present in both the hot and cold TSUNAMI cases to maintain consistency when computing Hot-to-Cold uncertainties. Note that the corresponding additional uncertainty curve does not approach 0.0 for low burnups as one expects from the definition of reactivity decrement. An alternate interpretation of this data is to use the 0.5 GWd/T step as the reference for "zero" burnup, as displayed in the bottom red curve of Figure 15 and in the central portion data of Table 2. This curve's shape trends towards 0.0 at zero burnup. With 0.5 GWd/T as the "zero" burnup reference, xenon is consistently represented in all data used to decompose the additional burnup uncertainty. Consequently, we choose to use the maximum uncertainty from any of the five lattices of Table 2 (at each burnup step) as the appropriate hot-to-cold uncertainty versus burnup, as is displayed in the bottom row of Table 2.

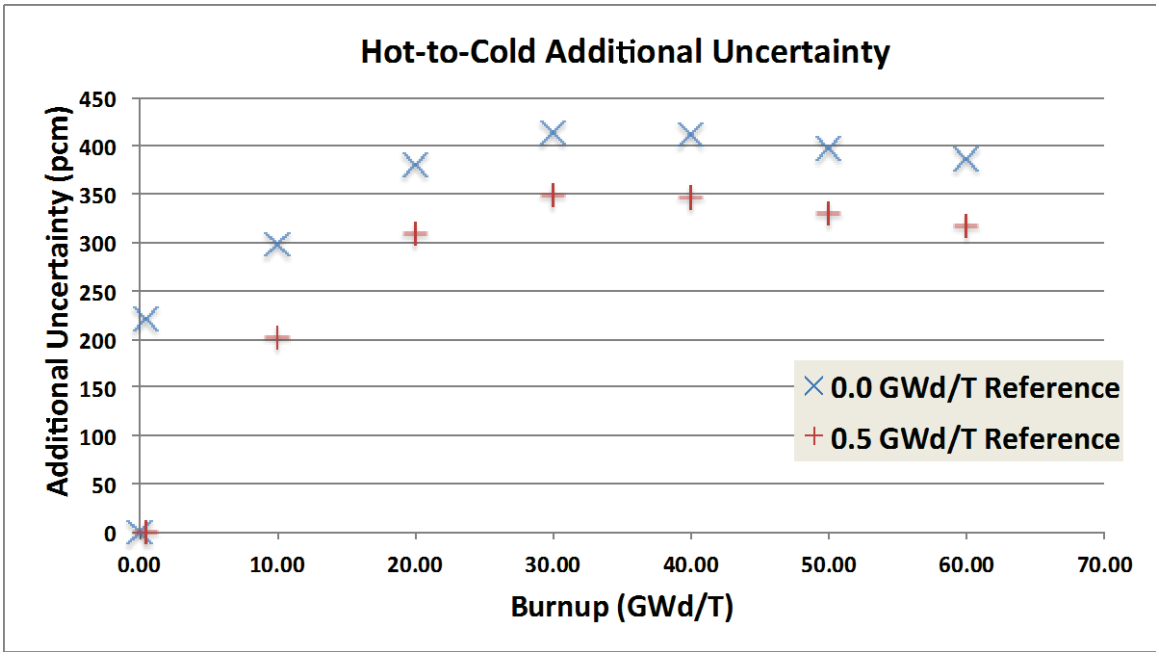

Figure 15 burnup Dependence of Hot-to-Cold Additional Uncertainties

With the fuel temperature and Hot-to-Cold additional uncertainties in hand, the complete rollup of uncertainties can be performed using the quadratic regression prediction interval widths and the 1.074 Tolerance Limit Factor, to arrive at a total uncertainty in pcm, as displayed in column 6 of Table 3.

Table 3 Rollup of Burnup Reactivity Decrement Bias Uncertainties

Reactivity Decrement Bias Uncertainty Rollup (in pcm) and Tolerance Limits of Bias in % of EPRI Lattice Cold Burnup Decrements							
GWd/T	HtoC	Fuel Temp	P.I. Width	T.L. Width	Tolerance Limit (pcm)	5% of Reactivity Decrement	T.L. in %
10	200	146	226	243	347	573	3.0
20	342	151	420	451	586	1011	2.9
30	349	131	585	628	731	1403	2.6
40	346	130	713	766	850	1772	2.4
50	330	162	812	872	946	2119	2.2
60	316	207	875	940	1013	2434	2.1
2-Sided 95/95 Tolerance Limit Factor = 1.074							

The uncertainty of measured reactivity decrement Tolerance Limits documented in this memo can be compared with the corresponding 95% uncertainty data for Table 1-2 of the original EPRI report [1], as reproduced here. The new WLS prediction-interval-based uncertainties are smaller at low burnups than the original report values, but they become nearly twice as large at high burnup.

Table 1-2
Measured Cold Reactivity Decrement Bias and Uncertainty

Burnup (GWd/T)	10.0	20.0	30.0	40.0	50.0	60.0
CASMO-4 Bias (pcm)	81	140	178	196	192	167
CASMO-5 Bias (pcm)	19	46	81	125	177	238
95% Uncertainty (pcm)	521	576	571	560	544	534

It is useful to convert the reactivity decrement uncertainty from pcm to a percentage of depletion reactivity in order to facilitate its ultimate application in applicants' LAR submittals to NRC (analogous with use of the Kopp 5%). It is important to remember that cold depletion reactivities and uncertainties (in pcm) are smaller in-rack than out-of-rack, as reported in the original EPRI report Tables 8-7 and 8-8 and reproduced here.

Table 8-7 HFP to Cold Uncertainty Matrix (2-sigma) at Cold Conditions

		Burnup (GWd/T)							
		0	0.5	10	20	30	40	50	60
Base	Reactivity (pcm)	9867	11843	11425	12605	13919	14986	15891	16527
	Uncertainty	347	427	459	508	527	530	521	509
128 IFBA 24 WABA	Reactivity (pcm)	9977	11927	11367	12556	13916	15009	15888	16612
	Uncertainty	337	403	450	508	533	531	521	512
3.50 % Enrichment	Reactivity (pcm)	12703	14810	13078	14402	15525	16266	16734	17034
	Uncertainty	365	437	498	555	550	537	518	500
4.25 % Enrichment	Reactivity (pcm)	11069	13112	12209	13469	14747	15699	16415	16931
	Uncertainty	350	434	473	529	540	534	520	508
Small Fuel Radius	Reactivity (pcm)	10205	12262	11602	12658	13981	14991	15849	16473
	Uncertainty	322	402	442	497	524	518	509	492

Table 8-8 HFP to Cold Uncertainty Matrix (2-sigma) in Rack Geometry

		Burnup (GWd/T)							
		0	0.5	10	20	30	40	50	60
Base	Reactivity (pcm)	-10145	-8018	-6291	-4658	-4002	-4097	-4601	-5344
	Uncertainty	222	287	324	353	358	356	349	339
128 IFBA 24 WABA	Reactivity (pcm)	-10405	-8323	-6684	-4858	-4094	-4130	-4626	-5347
	Uncertainty	212	274	317	352	364	354	346	341
3.50 % Enrichment	Reactivity (pcm)	-12437	-9905	-7382	-5715	-5839	-6687	-7688	-8688
	Uncertainty	204	266	330	364	357	349	343	337
4.25 % Enrichment	Reactivity (pcm)	-11101	-8772	-6740	-5028	-4684	-5123	-5916	-6873
	Uncertainty	211	279	327	357	359	350	342	337
Small Fuel Radius	Reactivity (pcm)	-10594	-8366	-6705	-5185	-4676	-5046	-5851	-7075
	Uncertainty	201	274	315	348	356	345	336	327

Since all of the uncertainty components computed in this memo are for cold out-of-rack conditions, an apples-to-apples conversion of units to **percent of depletion reactivity** must be made with cold **out-of-rack** depletion reactivities. For this purpose, we use the measured reactivity decrements for the seven nominal lattices that are depleted, branched to cold, and cooled for 100 hours (taken from Appendix C, Table C-3 of the original EPRI report [1]) as displayed in Table 4.

Table 4 Measured Cold Reactivity Decrements (Δk) for the Nominal EPRI Lattices

	Measured Reactivity Decrement					
Case	10	20	30	40	50	60
1	-0.1329	-0.2339	-0.3211	-0.3956	-0.4554	-0.5002
2	-0.1146	-0.2021	-0.2806	-0.3545	-0.4238	-0.4867
3	-0.1223	-0.2157	-0.2990	-0.3758	-0.4445	-0.5029
4	-0.1207	-0.2176	-0.3075	-0.3931	-0.4715	-0.5385
5	-0.2045	-0.2335	-0.2998	-0.3717	-0.4372	-0.4932
6	-0.1736	-0.2215	-0.2968	-0.3726	-0.4418	-0.5009
7	-0.2524	-0.2418	-0.2981	-0.3686	-0.4343	-0.4910

Column 7 of Table 3 contains **5% of the minimum of the seven lattice cold reactivity decrements** from Table 4 as a function of burnup, and column 8 of Table 3 displays the reactivity decrement bias uncertainty converted to a percentage of the out-of-rack cold depletion reactivity. It is important to remember that any conversion using LAR data would introduce an apples-to-oranges comparison, since LARs necessarily employ in-rack calculations

that have much lower depletion reactivity decrements. **Once conversion to percentage units has been done, only then is it appropriate to apply depletion decrement uncertainties directly to in-rack calculations.**

It is also more appropriate to use a 1-sided 95/95 Tolerance Limit (rather than the 2-sided limit used in Table 3) because one need not be concerned with data outside the 95/95 bands in the conservative direction. The 1-sided 95/95 Tolerance Limit Factor for 270 data points is 0.918 (e.g. k_1=1.807) while the 2-sided 95/95 Tolerance Limit Factor is 1.074 (e.g. k_2=2.114) for a 95% Student's t-value of 1.969. When the 1-sided Tolerance Limit is employed the column 5 data of Table 3 is reduced by ~17%, and the final rollup of results are displayed in Table 5. The maximum percentage tolerance limit of burnup reactivity decrement bias is 2.8% at 10.0 GWd/T.

Table 5 Rollup of Burnup Reactivity Decrement Bias Uncertainties (1-Sided Tolerance)

Reactivity Decrement Bias Uncertainty Rollup (in pcm) and Tolerance Limits of Bias in % of EPRI Lattice Cold Burnup Decrements							
GWd/T	HtoC	Fuel Temp	P.I. Width	T.L. Width	Tolerance Limit (pcm)	5% of Reactivity Decrement	T.L. in %
10	200	146	226	207	323	573	2.8
20	342	151	420	386	537	1011	2.7
30	349	131	585	537	654	1403	2.3
40	346	130	713	655	752	1772	2.1
50	330	162	812	745	831	2119	2.0
60	316	207	875	803	888	2434	1.8
1-Sided 95/95 Tolerance Limit Factor =			0.918				

From these results, one observes that **burnup reactivity decrement bias uncertainties (i.e., Tolerance Limits) are significantly smaller than 5.0% of depletion reactivity at all fuel assembly burnups.**

Moreover, the data presented here support the conclusion that **the EPRI burnup reactivity bias uncertainties are under 3.0% of depletion reactivity for all fuel assembly burnups.**

The final CASMO-5 depletion reactivity decrement bias and uncertainties from the WLS quadratic regression of sub-batch/cycle-collapsed biases (corresponding to Table 1-2 of the original EPRI report) are presented in Table 6, both in units of pcm and % of depletion reactivity decrement.

Table 6 Final Reactivity Decrement Bias and Uncertainty

CASMO-5 Measured Cold Reactivity Decrement Bias and Uncertainty						
Burnup (GWd/T)	10	20	30	40	50	60
Bias (pcm increase in k-eff)	66	101	106	80	22	-64
95/95 Tolerance Limit of Bias (pcm)	323	537	654	752	831	888
Bias (% Decrease in Reactivity Decrement)	0.6	0.5	0.4	0.2	0.1	-0.1
95/95 Tolerance Limit of Bias (%)	2.8	2.7	2.3	2.1	2.0	1.8

The original EPRI report will soon be updated to include the revised reactivity decrement biases and uncertainties, as summarized in this memo.

References

1. K. S. Smith et al., "Benchmarks for Quantifying Fuel Reactivity Depletion Uncertainty," Technical Report 1022909, EPRI, Palo Alto, CA, (2011).